Cell, Vol. 109, 397–407, May 3, 2002, Copyright ©2002 by Cell Press

# TRPM4 Is a $Ca^{2+}$-Activated Nonselective Cation Channel Mediating Cell Membrane Depolarization

**Pierre Launay,[1,5] Andrea Fleig,[2,5] Anne-Laure Perraud,[3] Andrew M. Scharenberg,[3] Reinhold Penner,[2,4] and Jean-Pierre Kinet[1]**
[1]Department of Pathology
Beth Israel Deaconess Medical Center
Harvard Medical School
Boston, Massachusetts 02215
[2]Laboratory of Cell and Molecular Signaling
Center for Biomedical Research
The Queen's Medical Center
John A. Burns School of Medicine
University of Hawaii
Honolulu, Hawaii 96813
[3]Department of Pediatrics and Immunology
University of Washington
Seattle, Washington 98195

## Summary

**Calcium-activated nonselective (CAN) cation channels are expressed in various excitable and nonexcitable cells supporting important cellular responses such as neuronal bursting activity, fluid secretion, and cardiac rhythmicity. We have cloned and characterized a second form of TRPM4, TRPM4b, a member of the TRP channel family, as a molecular candidate of a CAN channel. TRPM4b encodes a cation channel of 25 pS unitary conductance that is directly activated by $[Ca^{2+}]i$ with an apparent $K_D$ of ~400 nM. It conducts monovalent cations such as $Na^+$ and $K^+$ without significant permeation of $Ca^{2+}$. TRPM4b is activated following receptor-mediated $Ca^{2+}$ mobilization, representing a regulatory mechanism that controls the magnitude of $Ca^{2+}$ influx by modulating the membrane potential and, with it, the driving force for $Ca^{2+}$ entry through other $Ca^{2+}$-permeable pathways.**

## Introduction

The molecular characterization of the genes encoding the "transient receptor potential" (TRP) cation channels found in *Drosophila melanogaster* photoreceptors gave rise to a systematic cloning strategy for mammalian isoforms. Using expressed sequence tag (EST) and genomic database searches, at least 20 mammalian TRP-related genes have been cloned and the resulting channels extensively characterized (Harteneck et al., 2000; Hofmann et al., 2000; Clapham et al., 2001; Elliott, 2001; Montell et al., 2002b). In a recent unified nomenclature (Montell et al., 2002a), superseding the one proposed by Harteneck et al. (2000), TRP-related channels have been divided into three main subfamilies: TRPC for canonical TRP channels (previously STRPC), TRPV for those that are homologous for the archetypal vanilloid receptor (previously OTRPC), and TRPM for those with homology to the archetypal melastatin (previously LTRPC). All these proteins encompass six putative transmembrane domains and a slightly hydrophobic pore-forming region, while both N- and C-terminal domains are intracytoplasmic. Despite these similarities of structure, the functions of TRP channels are very different from one channel to another, even amongst the members of the same subfamily. It seems that each channel has specific ion selectivity and a particular mechanism of activation. Recently, three TRPM channels have been cloned and characterized electrophysiologically. Two of them, TRPM2 and TRPM7 (previously LTRPC2 and LTRPC7), contain enzymatic domains in the C-terminal intracellular portion of the channel (Nadler et al., 2001; Perraud et al., 2001; Runnels et al., 2001; Sano et al., 2001). At least for TRPM2, it appears that the nucleotide pyrophosphatase domain is responsible for ADP-ribose-mediated gating of the channel, whereas TRPM7 is regulated by cytoplasmic levels of Mg·ATP and the role of its kinase domain is less clear. A third TRPM channel, TRPM8, lacks an enzymatic domain and appears to be activated by low temperature and menthol (McKemy et al., 2002; Peier et al., 2002).

Although the channel activity of several TRP proteins, including TRPC3, TRPV5 (ECaC), TRPV6 (CaT1), TRPM2 (LTRPC2), and TRPM7 (LTRPC7), is affected either positively or negatively by changes in $[Ca^{2+}]i$, this effect is modulatory in nature, and there is so far no candidate TRP protein that has been shown to be directly gated by increases in $[Ca^{2+}]i$. Yet, there are numerous studies that have identified calcium-activated nonselective (CAN) cation channels in various tissues, including excitable and nonexcitable cells (Siemen, 1993; Thorn and Petersen, 1993; Partridge et al., 1994). CAN channels are directly activated by elevations in cytoplasmic $Ca^{2+}$ and they support large inward currents carried primarily by $Na^+$. Thus, their main function appears to mediate membrane depolarization, supporting important cellular responses such as neuronal bursting activity, kidney cell osmotic regulation, pancreatic acinar fluid secretion, and cardiac rhythmicity (Siemen, 1993; Thorn and Petersen, 1993; Partridge et al., 1994). One remarkable feature of these channels is that they do not seem to undergo voltage- or $Ca^{2+}$-dependent inactivation and therefore are capable of maintaining membrane depolarization. Thus far, the basis for the identification of CAN channels rests in the details of electrophysiological characterizations in various cell types, while the molecular identity of these channels remains a mystery.

Here we report a TRPM channel, designated TRPM4b, which does not contain any obvious enzymatic domain. However, TRPM4b has the distinct properties of a CAN channel. This channel is specific for monovalent cations and is strictly activated by calcium as assessed by single-channel recording. Since TRPM4b does not carry any significant $Ca^{2+}$, its main function appears to provide a mechanism that allows cells to depolarize in a $Ca^{2+}$-dependent manner. In nonexcitable cells that lack voltage-dependent $Ca^{2+}$ channels, this depolarization would decrease the driving force for $Ca^{2+}$ influx through store-

[4]Correspondence: rpenner@hawaii.edu
[5]These authors contributed equally to this work.

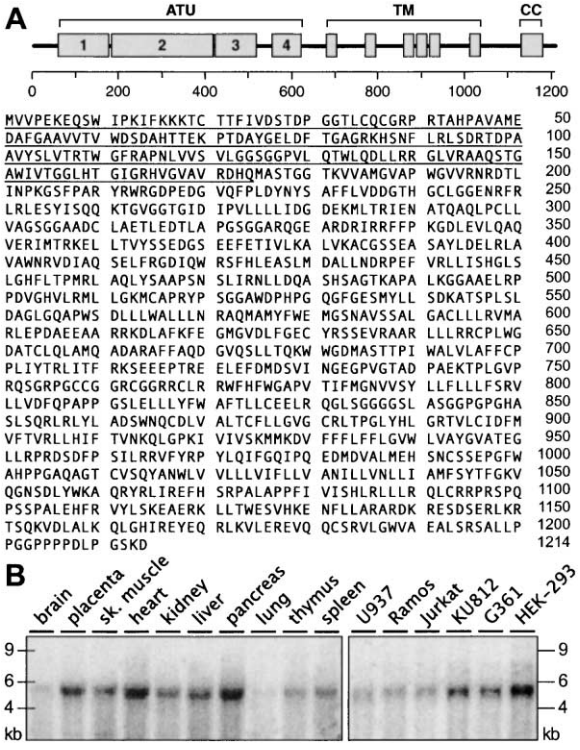


Figure 1. Molecular Characterization of TRPM4b

(A) Schematic and primary structure of TRPM4b with amino-terminal unique region 1-4 (ATU), transmembrane domain regions (TM), coiled-coil region (CC). Underlined amino acids represent the N-terminal extension of TRPM4b; the rest of the sequence is identical to the short splicing variant TRPM4.

(B) Northern blot analysis of RNA from various tissues and human cell lines using a specific TRPM4b antisense RNA probe. Cell lines represent monocytes (U937), B lymphocytes (Ramos), T lymphocytes (Jurkat), basophils (Ku812), melanoma cells (G361), and embryonic kidney cells (HEK-293).

operated $Ca^{2+}$ channels, whereas in excitable cells this channel could be important to shape action potential duration and spiking frequency. Since TRPM4b is widely expressed and is detected endogenously after receptor-activated calcium entry, we propose that TRPM4b is a CAN channel involved in cell depolarization.

## Results

### Isolation of TRPM4 Gene

To identify putative cation channels, we used a fragment of a human EST 1076485 cDNA that showed similarity to TRPM2, and we screened fetal kidney, spleen, and prostate adenocarcinoma cDNA libraries to obtain a full 4062 base pair coding sequence for the transcript subsequently designated TRPM4b according to a recently proposed nomenclature (Montell et al., 2002a). This TRPM family member is characterized by the following structural elements: four domains in the amino-terminal unique region (ATU) that are homologous among all members of the TRPM subfamily, six transmembrane spanning domains (TM), and a region with predicted coiled-coil character (CC) at the C-terminal end (Figure 1A). The predicted primary structure of TRPM4b revealed a 1214 amino acid protein that is nearly identical to a previously reported TRPM4 protein (Xu et al., 2001), except that the present predicted protein includes an additional 174 amino acids N-terminal to the predicted start of Xu et al.'s TRPM4 protein (Figure 1A). The latter is the result of an alternative splicing of the gene with the third and fourth exons being spliced out and the beginning of the first exon being truncated. As a consequence, the first in-frame methionine lies in the fifth exon, resulting in the deletion of the first 174 amino acids. Hence, we propose that the Xu et al. protein be designated TRPM4a and the longer protein described here TRPM4b. Northern blot analysis indicates that an approximately 4–5 kb band, possibly representing a combination of TRPM4a and TRPM4b transcripts, is widely expressed in various tissues with a dominant expression in the heart, placenta, and pancreas (Figure 1B). This 4–5 kb band is also detected in spleen and thymus, albeit at lower levels. To corroborate this result on cells derived from these organs, the same probe was used to assess the expression of TRPM4 transcripts in hematopoetic cell lines. As illustrated in Figure 1B, endogenous TRPM4 transcripts were detected in all cell lines tested, including B and T lymphocytes as well as monocytes, basophils, and kidney-derived HEK-293 cells.

### TRPM4b Is Expressed at the Cell Surface

Because we were not able to identify a cell line lacking endogenous TRPM4 transcript expression, we chose the HEK-293 cellular system for overexpression of TRPM4b based on its suitability for tetracycline-controlled expression and its well-established use in the expression and characterization of other ion channels, including TRPM2 and TRPM7. In order to characterize TRPM4b, we established stable HEK-293 clones in which TRPM4b expression is under control of a tetracycline-regulated promotor. For biochemical analysis, TRPM4b was Flag tagged in the N-terminal region and, as shown in Figure 2A, its overexpression is easily detectable after immunoprecipitation with an anti-Flag antibody when cells were treated for 18 hr with tetracycline. However, no TRPM4b protein was detected after either immunoprecipitation with an irrelevant control antibody (Ctrl) or when the cells were not exposed to tetracycline (Figure 2A). To assess further molecular and functional features, the cell surface expression of TRPM4b was studied by surface labeling with iodine. HEK-293 cells overexpressing TRPM4b were radioactively labeled before lysis, and the immunoprecipitated samples were split so that half of the samples were subject to an autoradiography. After anti-Flag immunoprecipitation the protein was detected as a single band corresponding to TRPM4b (Figure 2B). As a control for iodine surface labeling, the other half of the samples was blotted using an anti-Cbl antibody showing that the 120 kDa intracytoplasmic Cbl protein is present in the cell lysate (Figure 2B, right) but not detectable by autoradiography. Thus, TRPM4b is expressed as a plasma membrane protein.

### TRPM4b Can Homoassociate

Since most ion channels require tetrameric arrangement of multiple transmembrane spanning domains to form

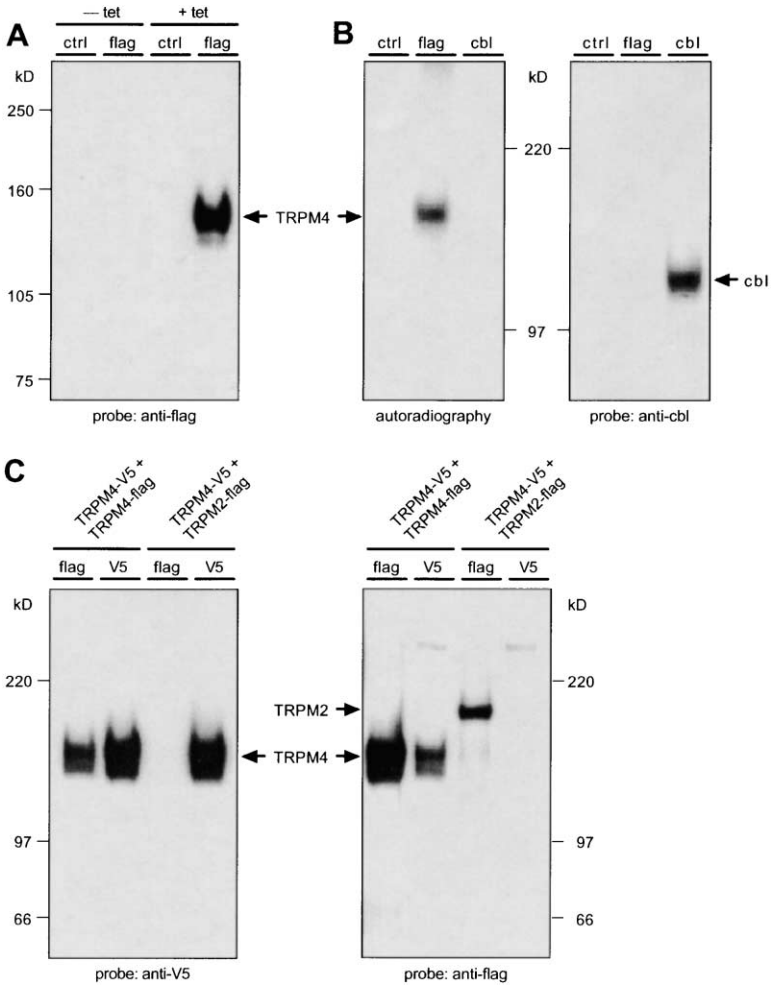


Figure 2. Biochemical Analysis of TRPM4

(A) Tetracycline-inducible expression of TRPM4b. Stable TRPM4b HEK-293 clones were treated or not for 18 hr with 1 μg/ml of tetracycline. Clones were analyzed for expression of a Flag-reactive protein by anti-Flag immunoprecipitation/anti-Flag immunoblotting. Ctrl indicates immunoprecipitation with an irrelevant antibody.

(B) Surface expression of TRPM4b. Surface proteins of tetracycline-induced clones were labeled with iodine. TRPM4b was immunoprecipitated with the Flag antibody; the cell viability was tested by immunoprecipitation of the intracytoplasmic protein Cbl.

(C) TRPM4b homomultimerization. HEK-293 cells were cotransfected with two different tagged forms (V5 and Flag) of TRPM4b or cotransfected with TRPM4b V5-tagged and TRPM2 Flag-tagged. Cell lysates were immunoprecipitated with Flag and V5, and Western blots of the immune complexes were probed with both anti-V5 and anti-Flag antibodies.

a proper pore structure, we used a biochemical approach to assess the homomultimerization of TRPM4b. To this end, HEK-293 cells were cotransfected with both Flag-tagged TRPM4b or TRPM2 and V5-tagged TRPM4b. The cell lysate was separated into two equal amounts, and the TRPM4b molecules were immunoprecipitated with both the Flag and the V5 antibodies. Samples were then separated for different Western blots with either the Flag antibody or the V5 antibody. When HEK-293 cells were transfected with the two different tagged forms of TRPM4b, the immunoprecipitated V5-TRPM4b coprecipitated with the Flag-tagged TRPM4b and vice versa (Figure 2C). In contrast, control Flag-TRPM2 did not coprecipitate with V5-TRPM4b. Therefore, we conclude that TRPM4b can homoassociate, consistent with the hypothesis that homomultimeric TRPM4b channels would be important contributors to TRPM4b function in a cellular context.

### TRPM4b Is a $Ca^{2+}$-Activated Cation Channel

Based on its homology to other members of the TRPM family of proteins, three of which have now been characterized as cation channels, we surmised that TRPM4b would also form a cation channel with its open probability likely to be regulated by an intracellular molecule. To test this, we performed patch-clamp analyses of plasma-membrane currents in TRPM4b overexpressing HEK-293 cells. Since the amino acid sequence of TRPM4b did not reveal any obvious clues as to what might be the activating mechanism for this putative ion channel, and since we failed to observe any constitutive ion channel activity in HEK-293 cells overexpressing TRPM4b, we initially screened for mechanisms that have previously been shown to gate cation channels in either native or overexpression systems. The stimuli we tested included cyclic nucleotides (cAMP, cGMP), ADP-ribose, store depletion by $InsP_3$, and receptor stimulation. However, none of these stimuli was adequate to gate TRPM4b under experimental conditions in which intracellular $Ca^{2+}$ levels were buffered at or below 100 nM (data not shown).

Since a number of cell types have been reported to express $Ca^{2+}$-activated cation channels (Siemen, 1993; Thorn and Petersen, 1993; Partridge et al., 1994), we next tested for a possible $Ca^{2+}$-dependent activation mechanism by perfusing cells with defined $[Ca^{2+}]i$ between 0.3 and 1 μM, which were established by appropriate mixtures of BAPTA and $CaCl_2$. As illustrated in Figure 3A, elevated levels of $[Ca^{2+}]i$ were indeed successful in activating large currents in cells overexpressing TRPM4b. Immediately following establishment of the whole-cell configuration, $[Ca^{2+}]i$ levels of 0.3–1 μM

induced large inward and outward currents at −80 mV and +80 mV, respectively. These currents activated rapidly, i.e., within 2–4 s, and peaked around 10 s into the experiment. The current-voltage relationship of the $Ca^{2+}$-induced current is illustrated in Figure 3B and is characterized by slight inward rectification at negative and somewhat more pronounced outward rectification at positive voltages.

As illustrated in Figure 3A, the magnitude of currents was dependent on the level of $[Ca^{2+}]i$. In addition, the current magnitude was also dependent on the time that cells were incubated with tetracycline, where longer incubation times yielded larger currents, consistent with a time-dependent accumulation of expressed TRPM4b proteins in the plasma membrane. A comprehensive assessment of TRPM4b-dependent currents as a function of $[Ca^{2+}]i$ is illustrated in Figure 3C for cell populations that were exposed to tetracycline for 18–22 hr and 24–28 hr. The dose-response curves fitted to these data yield $IC_{50}$ values of 320 nM (18–22 hr tetracycline exposure) and 520 nM (24–28 hr tetracycline incubation), respectively. Both curves are characterized by a rather high cooperativity (Hill coefficient = 6 and 4, respectively). At −80 mV, the average peak amplitudes of inward currents obtained with $[Ca^{2+}]i \geq 800$ nM was $-742 \pm 166$ pA (n = 6) in cells that were exposed to tetracycline for 18–22 hr. This represents a larger than 5-fold increase in $Ca^{2+}$-activated currents compared to either uninduced HEK-293 cells (i.e., stably transfected with TRPM4b but not exposed to tetracycline), which generate $-114 \pm 47$ pA (n = 10), or wt HEK-293 cells, which express endogenous TRPM4b levels that amount to average inward currents of $-142 \pm 67$ pA (n = 6; see Figure 5). In cells that were incubated with tetracycline for 24–28 hr, inward currents increased to an average of $-3.1 \pm 0.5$ nA (n = 9), corresponding to a >20-fold increase over wt controls.

### TRPM4b Is Activated by $Ca^{2+}$-Mobilizing Receptor Agonists

From the above experiments, TRPM4b appears to represent a $Ca^{2+}$-activated nonspecific cation channel and, under more physiological conditions, would be expected to activate following receptor stimulation with agonists that couple to $InsP_3$ production, as this leads to $Ca^{2+}$ release from intracellular stores and subsequent activation of store-operated $Ca^{2+}$ influx (Parekh and Penner, 1997). We tested this hypothesis in HEK-293 cells overexpressing TRPM4b by performing voltage-clamp experiments in which we measured membrane currents and $[Ca^{2+}]i$ simultaneously following ATP-mediated stimulation of endogenous purinergic receptors, presumably $A_{2B}$ and $P2Y_2$ receptors coupling to phospholipase C through $G_{q11}$ (Gao et al., 1999). As in the previous experiments, whole-cell currents were continuously monitored by voltage ramps. However, here we did not buffer $[Ca^{2+}]i$ to fixed levels, but instead left $[Ca^{2+}]i$ to vary freely, and we monitored the changes in $[Ca^{2+}]i$ by fura-2. In addition, we chose a more negative holding potential of −60 mV in order to provide significant driving force for $Ca^{2+}$ influx.

Figure 3D represents a typical experiment under such experimental conditions (n = 8), illustrating that application of extracellular ATP induced a large transient increase in $[Ca^{2+}]i$ that was followed by waves of smaller $Ca^{2+}$ oscillations, likely due to store-operated $Ca^{2+}$ influx (bottom trace). The middle graph plots the corresponding inward currents at −80 mV as a function of time, revealing that the large initial $Ca^{2+}$ transient was relatively ineffective at activating TRPM4b. However, significantly larger inward currents were activated during the secondary phase of oscillatory changes in $[Ca^{2+}]i$, suggesting that $Ca^{2+}$-influx-mediated, localized elevations of $[Ca^{2+}]i$ underneath the plasma membrane are more efficient in triggering TRPM4b activity than global cytosolic $Ca^{2+}$ transients resulting from $Ca^{2+}$ release. Note, however, that the current amplitudes during the $[Ca^{2+}]i$ oscillations are not absolutely correlated with the global cytosolic levels of $[Ca^{2+}]i$, suggesting that some of the TRPM4b channels may colocalize with store-operated influx channels and may therefore be more accessible to $Ca^{2+}$-dependent activation. Typical current-voltage relationships obtained prior to ATP stimulation and during the transient activation of TRPM4b are illustrated in Figure 3E. Since the TRPM4b-mediated currents reverse at ~0 mV (Figure 3E), enhanced activity of TRPM4b would tend to depolarize cells from a rather negative resting membrane potential, which is largely determined by resting and/or $Ca^{2+}$-dependent $K^+$ conductances. To visualize the impact of TRPM4b activation on the cell's membrane potential, we determined the reversal potential of each current trace elicited by our voltage ramp protocol and plotted it as a function of time (top graph of Figure 3D). As can be seen, the oscillatory activity of TRPM4b translates into oscillatory changes in reversal potential, which would alternatingly hyper- and depolarize the cell's membrane potential. Such oscillations in membrane potential will significantly affect $Ca^{2+}$ influx, since negative potentials will increase and depolarized potentials will decrease the driving force for $Ca^{2+}$ entry.

### Single-Channel Properties of TRPM4b

An important question arising from the above experiments is whether the $[Ca^{2+}]i$-mediated activation of TRPM4b is a direct consequence of $Ca^{2+}$ binding to the channel or due to secondary $Ca^{2+}$-dependent signaling pathways. We addressed this issue by studying single-channel activities in cell-free excised membrane patches in the inside-out configuration of the patch-clamp technique. Figure 4A illustrates a representative experiment (n = 5) in which a membrane patch containing at least 5 TRPM4b channels was initially excised in the inside-out configuration into a $Ca^{2+}$-free NaCl-based solution that additionally contained 1 mM EDTA (patch excision is marked by the arrow). The patch remained quiet until the cytosolic side of the patch was exposed to a K-glutamate-based solution in which $Ca^{2+}$ was buffered to 300 nM. We chose a K-glutamate-based solution to mimic the experimental conditions of our standard whole-cell experiments. Under these conditions, we consistently observed activity of multiple channels while the cytosolic side of the patch was exposed to elevated $Ca^{2+}$ and channel activity rapidly subsided as $Ca^{2+}$-free solution was reintroduced.

Figure 4B illustrates typical single-channel recordings at various membrane potentials obtained from isolated

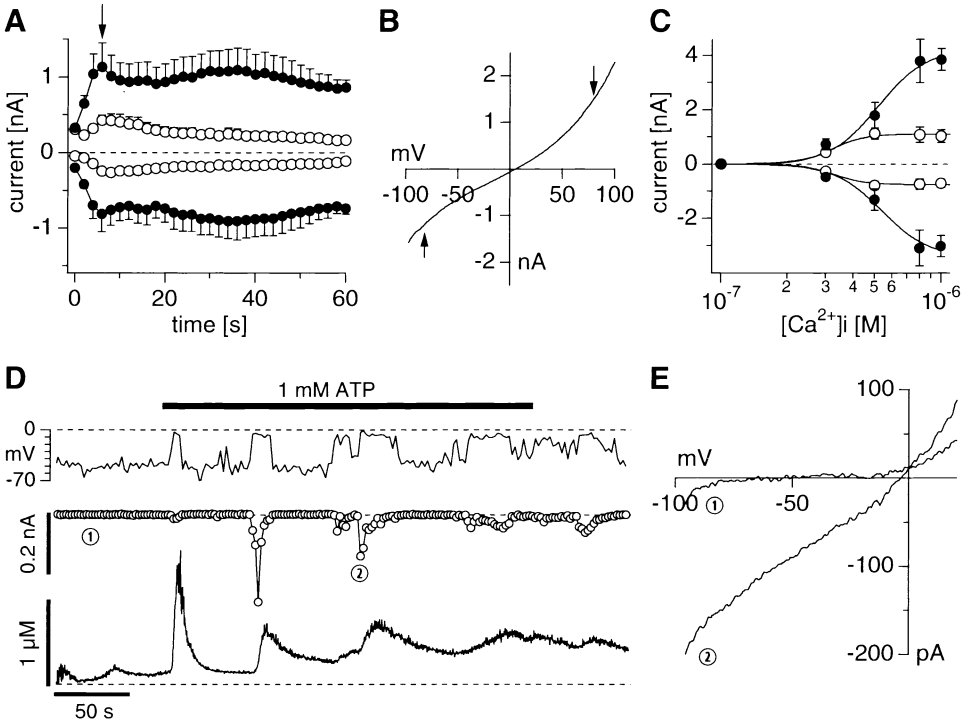


Figure 3. Functional Expression of TRPM4b in HEK-293 Cells

(A) Whole-cell recordings in HEK-293 cells overexpressing TRPM4b. Average inward and outward currents carried by TRPM4b at −80 and +80 mV, respectively. Cells were perfused with solutions in which $[Ca^{2+}]i$ clamped to either 300 nM (closed circles, n = 5 ± SEM) or 500 nM (open circles, n = 5 ± SEM). Arrow indicates the time at which the raw data trace displayed in (B) was extracted.

(B) Current-voltage relationship under experimental conditions as in (A), obtained 8 s after whole-cell establishment from a representative cell perfused with 500 nM $[Ca^{2+}]i$. Arrows indicate −80 and +80 mV, respectively.

(C) Dose-response behavior of expressed TRPM4b to various intracellular calcium concentrations in populations of cells exposed to tetracycline for 18–22 hr (open circles) and 24–28 hr (closed circles). Data points represent average inward and outward currents at −80 and +80 mV, respectively, taken 8 s after whole-cell establishment (n = 3–12).

(D) Receptor-mediated activation of expressed TRPM4b. Traces represent concomitant measurements of global $[Ca^{2+}]i$ (bottom trace), whole-cell current (middle trace), and reversal potential ($E_{rev}$) (top trace) in a representative cell (total n = 8). For the time indicated, the cell was superfused with an extracellular solution containing 1 mM ATP. Holding potential was −60 mV to promote calcium influx. Note that TRPM4b current amplitude does not strictly follow changes in $[Ca^{2+}]i$, and the initial release transient is less effective at activating TRPM4b than the later phase of calcium influx. [1] and [2] indicate the time at which raw data traces displayed in (E) were extracted.

(E) Current-voltage relationships from the same cell as shown in (D). Both a control current trace before ATP challenge and a TRPM4b current trace (214 s after whole-cell establishment) are displayed.

patches whose cytosolic side was exposed to intracellular solutions in which $[Ca^{2+}]$ was buffered to 300 nM. Multiple TRPM4b channels were routinely observed in all experiments (16 out of 16 patches), whereas only 38% of wild-type HEK-293 cells showed similar $Ca^{2+}$-activated channels (3 out of 8 patches), and those that did contained fewer channels per patch. TRPM4 channel activity showed both an increase in open probability as well as an increase in open times at positive potentials, which may in part account for the slight outward rectification observed in whole-cell recordings. In addition, single-channel amplitudes exhibited slight rectification at both positive and negative membrane voltages (Figure 4C), which may account for the S-shaped appearance of both single-channel and whole-cell current-voltage relationships (cf. Figures 4C and 3B). The single-channel conductance was 25 pS as assessed by linear regression over the voltage range of −60 to +60 mV. In addition to the steady voltage protocol illustrated in Figure 3A, we also studied single-channel behavior in voltage ramps (Figure 4D), and the ensemble average of 129 current records (Figure 4E) revealed a similar overall current-voltage relationship as obtained in whole-cell recordings. The stronger outward rectification of the ensemble average patch currents compared with whole-cell currents is likely due to the length of the voltage ramp (5 s), which accentuates the voltage-dependent increase in open probability at positive potentials.

### TRPM4 Is Endogenously Expressed in HEK-293 Cells

Since TRPM4b is also natively expressed in HEK-293 cells, we wanted to assess the properties of endogenous $Ca^{2+}$-activated currents in wt HEK-293. Figure 5 illustrates that untransfected HEK-293 cells indeed express $Ca^{2+}$-dependent currents that are qualitatively indistinguishable from overexpressed TRPM4b currents. Thus, perfusing cells with 500 nM $[Ca^{2+}]i$ leads to activation of inward and outward currents measured at −80 mV and +80 mV, respectively (Figure 5A). The main difference compared with TRPM4b-overexpressing cells is the magnitude of the currents, which is on average

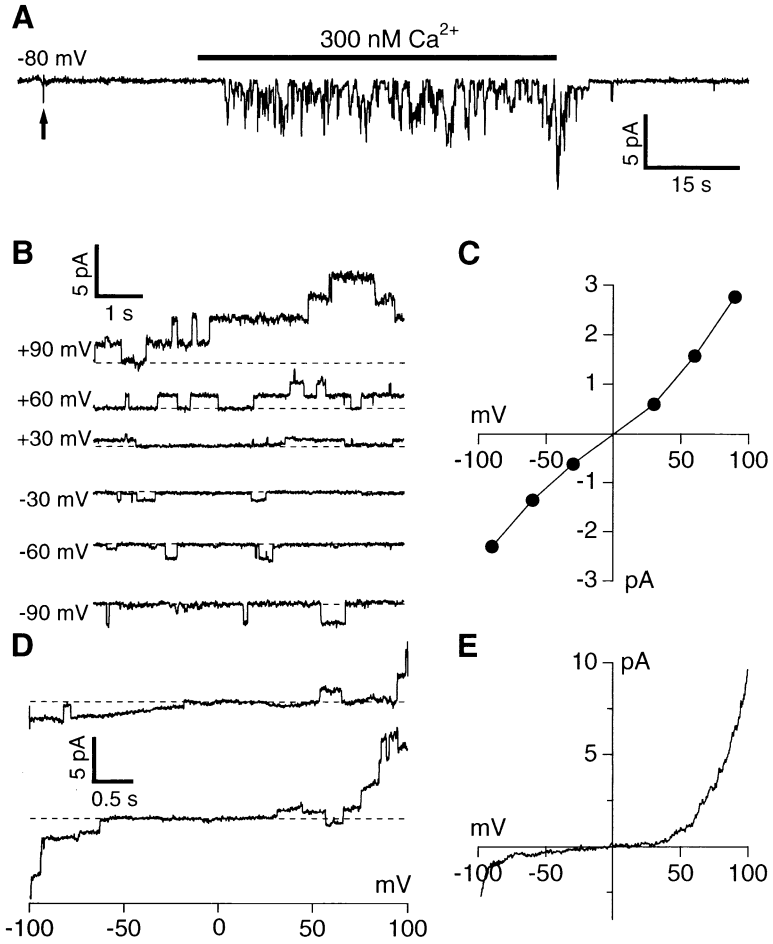


Figure 4. Single-Channel Properties of TRPM4b

(A) Reversible activation of TRPM4b channels by 300 nM [$Ca^{2+}$] recorded in inside-out patches excised from a TRPM4b-overexpressing HEK-293 cell. The patch was excised at the time indicated by the arrow into a NaCl-based solution in which [$Ca^{2+}$]i was initially buffered to zero ($Ca^{2+}$-free + 1 mM EDTA). During the time indicated by the bar, the inside of the patch was exposed to a K-glutamate-based solution, but with [$Ca^{2+}$] buffered to 300 nM. The pipette solution was a NaCl-based standard external solution. Channel activity was measured at −80 mV. Data are from a single representative patch out of five similar recordings.

(B) Activation of TRPM4b channels by 300 nM [$Ca^{2+}$] recorded in a typical inside-out patch excised from a TRPM4b-overexpressing HEK-293 cell. The patch was excised into a KCl-based solution in which [$Ca^{2+}$]i was buffered to 300 nM and the pipette solution was a NaCl-based standard external solution. Channel activity was measured at various membrane potentials as indicated. Data are from a single representative patch out of 16 successful recordings. Note that open probability increases with positive membrane voltage, and single-channel amplitudes slightly increase at both positive and negative potentials.

(C) Single-channel I-V relationship derived from averages of several events from different patches (n = 2–5), yielding a single channel conductance of 25 pS between −60 mV and +60 mV. Note rectification of single-channel amplitudes at positive and negative voltages.

(D) Two sample single-channel ramp recordings measured under the conditions as in (A). Ramps spanned −100 to +100 mV and were 5 s long.

(E) Cumulative average of 129 single-channel ramps (same patch as in [D]), consistent with the behavior of whole-cell currents carried by TRPM4b. Note the characteristic outward rectification and $E_{rev}$ around 0 mV.

about −142 ± 67 pA at −80 mV (n = 6) and therefore 5–20 times smaller than in cells overexpressing TRPM4b (see Figure 3). As a further control, we also measured $Ca^{2+}$-activated currents in HEK-293 cells that were exposed to tetracycline for 18–22 hr but were induced to express TRPM2, which is an ADP-ribose-gated channel that is not activated by $Ca^{2+}$ directly. These cells yielded average $Ca^{2+}$-induced inward currents of −100 pA ± 21 (n = 6, data not shown), which is similar to the levels found in either uninduced TRPM4b-transfected HEK-293 cells (−114 ± 47 pA, n = 10) or wt HEK-293 (−142 ± 67 pA, n = 6).

The kinetics of endogenous TRPM4b currents differ from those recorded from HEK-293 cells overexpressing TRPM4b in that there is a noticeable delay of ~10 s in the activation of wt currents compared with those carried by overexpressed channels. Possible reasons for such a delay might be due to a specialized localization of endogenous TRPM4b channels to membrane areas that are not as easily accessible to our internal solutions or the fact that they colocalize with $Ca^{2+}$ removal mechanisms such as pumps. Another possible reason could be that endogenous TRPM4b channels have regulatory elements that overexpressed channels do not possess. However, the current-voltage relationship of the endogenous TRPM4b current exhibits the same S-shaped form (Figure 5B), and the $Ca^{2+}$ dependence of activation is very similar to that seen in TRPM4b-overexpressing cells, with an $IC_{50}$ of 420 nM and a Hill coefficient of 6. Likewise, wt HEK-293 cells studied under the same conditions as those shown in Figure 3D (n = 8) responded similarly to receptor stimulation in that ATP-mediated oscillations in [$Ca^{2+}$]i were accompanied by activation of inward currents and characteristic shifts in reversal potential (Figure 5D). Moreover, current-voltage relationships under these experimental conditions (Figure 5E) exhibited the same features as those observed in the overexpressing cells. Together, these results indicate that the $Ca^{2+}$-dependent channels observed in wt HEK-293 cells are essentially identical to those observed in TRPM4b-overexpressing cells, but are less abundantly expressed.

### TRPM4b Is Specific for Monovalent Cations

An important question arising from the above experiments is whether TRPM4b is able to carry $Ca^{2+}$ ions, as this would potentially represent a mechanism of $Ca^{2+}$-induced $Ca^{2+}$ influx. We assessed this by experiments shown in Figures 6A and 6B, where TRPM4b was activated by 800 nM [$Ca^{2+}$]i while cells were bathed in the

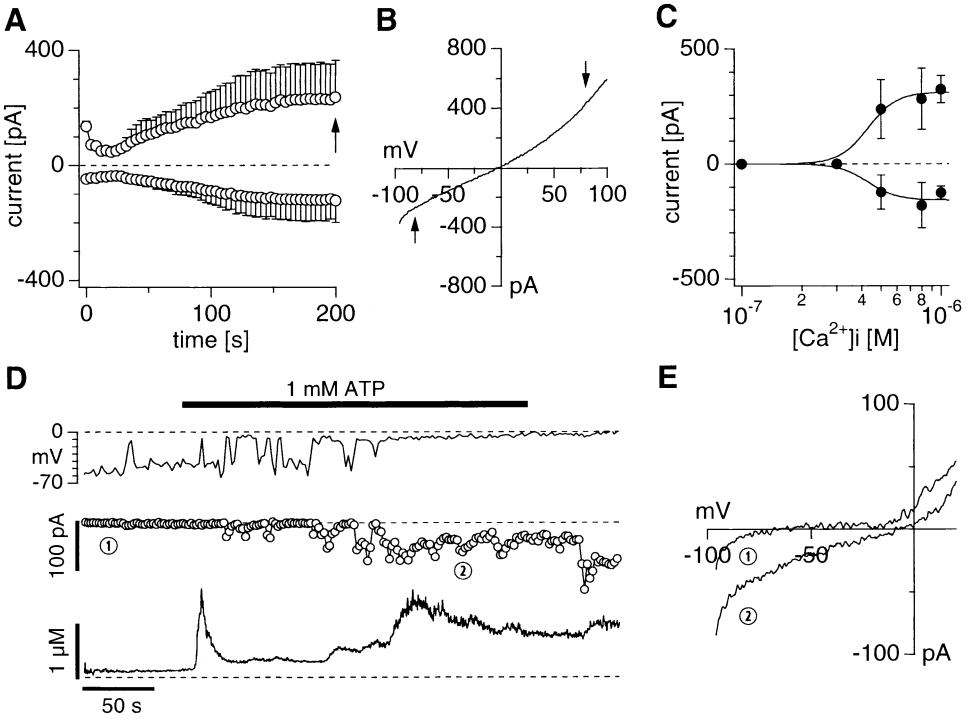


Figure 5. Endogenous TRPM4b-Like Currents in HEK-293 Cells

(A) Whole-cell recordings in wild-type HEK-293 cells perfused with solutions in which $[Ca^{2+}]i$ clamped to 500 nM (n = 3 ± SEM). Average inward and outward currents at −80 and +80 mV, respectively, carried by endogenous currents with TRPM4b characteristics. Arrow indicates the time at which the raw data trace displayed in (B) was extracted. Note that activation of endogenous TRPM4b-like current proceeds slightly slower than overexpressed TRPM4b.

(B) Current-voltage relationship under experimental conditions as in (A), obtained from a representative cell 200 s after whole-cell establishment. Arrows indicate −80 and +80 mV, respectively.

(C) Dose-response behavior of endogenous TRPM4b-like current to various intracellular calcium concentrations. Data points represent average inward and outward currents at −80 and +80 mV, respectively, taken 200 s after whole-cell establishment (n = 3 each).

(D) Receptor-mediated activation of endogenous TRPM4b-like current. Shown are concomitant measurements of global $[Ca^{2+}]i$ (bottom trace), whole-cell current (middle trace), and reversal potential ($E_{rev}$) (top trace) in a representative cell (total n = 8). For the time indicated, the cell was superfused with an extracellular solution containing 1 mM ATP. Holding potential was −60 mV to promote calcium influx. [1] and [2] indicate the time at which raw data traces displayed in (E) were extracted.

(E) Current-voltage relationships from the same cell as shown in (D). Both a control current trace before ATP challenge and TRPM4b-like current trace (286 s after whole-cell establishment) are displayed.

standard extracellular solution and subsequently exposed to isotonic $CaCl_2$ solution (120 mM). As can be seen in Figure 6A, this resulted in complete suppression of inward currents with no significant change in outward current. The current-voltage relationships under these conditions are illustrated in Figure 6B, demonstrating that the inward currents at negative potentials, initially carried by $Na^+$, are completely suppressed when exposing cells to isotonic $Ca^{2+}$. Note that in the absence of external $Na^+$, the reversal potential shifts to negative potentials (−75 mV), due to the absence of a depolarizing current carrier. Thus, TRPM4b channels do not carry any appreciable amount of $Ca^{2+}$ and can therefore be designated as $Ca^{2+}$-activated monovalent cation channels. This also suggests that the channels' main function may be to depolarize cells and thereby shape the driving force for $Ca^{2+}$ influx.

As a further test for the specificity of TRPM4b for monovalent cations, we performed experiments very similar to those described above. Here we also activated TRPM4b in TRPM4b-overexpressing HEK-293 cells by 800 nM $[Ca^{2+}]i$, but subsequently exposed them to a standard extracellular solution in which all but 1 mM NaCl was replaced by impermeant choline-Cl. As illustrated in the bottom graph of Figure 6C, this resulted in an almost complete block of the inward current through TRPM4b channels. As a result, the initial depolarization induced by the elevated $[Ca^{2+}]i$ of 800 nM was partially reversed by the choline-based solution (top graph of Figure 6C), since very little $Na^+$ remained to sustain a strong depolarization. The current-voltage relationships of whole-cell currents obtained immediately following break-in, after the peak of TRPM4b activation, and during choline-Cl exposure confirm that the reduction in $Na^+$ influx cause a hyperpolarizing shift in reversal potential (Figure 6D). As will be shown below, we took advantage of this effect to probe for the functional role of TRPM4b in shaping intracellular $Ca^{2+}$ signals.

### TRPM4b Decreases $Ca^{2+}$ Influx through Membrane Depolarization

Since TRPM4b does not carry significant $Ca^{2+}$ and its activation leads to a $Ca^{2+}$-dependent depolarization, we reasoned that receptor-mediated $Ca^{2+}$ signals might be negatively regulated by activation of TRPM4b, as a depolarization would decrease the driving force for $Ca^{2+}$

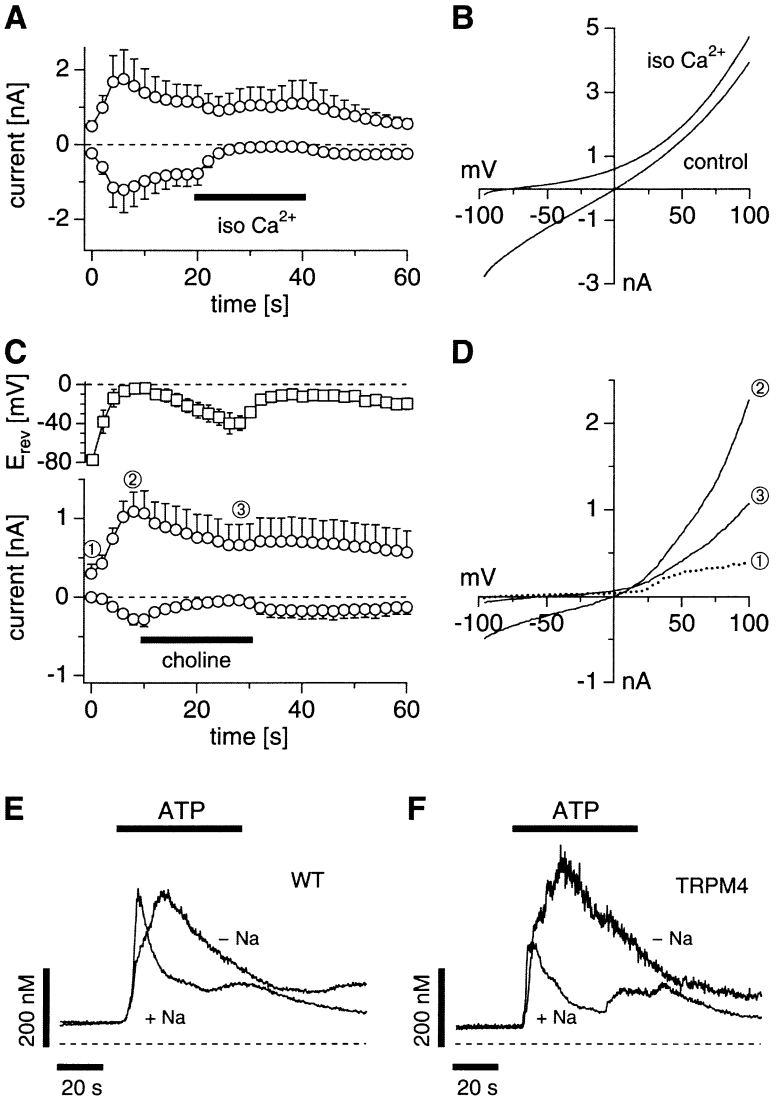


Figure 6. TRPM4b Does Not Carry $Ca^{2+}$ and Inhibits $Ca^{2+}$ Influx

(A) Whole-cell recordings in HEK-293 cells overexpressing TRPM4b. Average inward and outward currents carried by TRPM4b at −80 and +80 mV, respectively. Cells were perfused with solutions in which $[Ca^{2+}]i$ was buffered to 800 nM (n = 5 ± SEM). Cells were exposed to 120 mM isotone $CaCl_2$ as indicated by the black bar (300 mOsm). Note that inward currents are completely suppressed, suggesting that TRPM4b does not carry $Ca^{2+}$ ions.

(B) Current-voltage relationships of TRPM4b currents under experimental conditions as in (A) measured just before and during application of isotone $CaCl_2$ (40 s after whole-cell establishment). Note that isotone $CaCl_2$ application changes $E_{rev}$ to −75 mV and outward $K^+$ currents remain largely unaffected.

(C) Whole-cell recordings in HEK-293 cells overexpressing TRPM4b. Bottom: Average inward and outward currents carried by TRPM4b at −80 and +80 mV, respectively. Holding potential was −60 mV. Cells were perfused with solutions in which $[Ca^{2+}]i$ was buffered to 800 nM (n = 6 ± SEM). For the time indicated by the bar, cells were exposed to a choline-Cl-based solution that additionally contained 1 mM NaCl and 2.8 mM KCl. Symbols [1], [2], and [3] indicate the time at which raw data traces displayed in (D) were extracted. Top: Reversal potentials extracted from individual ramp current records. Note that initial activation of TRPM4b leads to depolarization, and choline application causes hyperpolarization.

(D) Current-voltage relationships of TRPM4b currents under experimental conditions as in (C) measured in an exemplary cell at the start of the experiment [1] and just before [2] and during [3] application of choline-Cl-based solution.

(E) Averaged $[Ca^{2+}]i$ signals in intact wt HEK-293 cells loaded with fura-2-AM and stimulated by the purinergic receptor agonist ATP (n = 7–10). During the time indicated by the bar, cells were exposed to 1 mM ATP in either $Na^+$-based (+ Na) or choline-based (− Na) extracellular solutions, as indicated by labels. (F) Same experimental protocol as in (E), except that the measurements were performed on TRPM4b-overexpressing HEK-293 cells (n = 8–11).

influx and thereby attenuate changes in $[Ca^{2+}]i$. As there are no known specific inhibitors of TRPM4b that would allow us to test this hypothesis pharmacologically, we took advantage of the high selectivity of TRPM4b for monovalent cations and addressed this hypothesis in intact cells in which we monitored $[Ca^{2+}]i$ following ATP-mediated changes in $[Ca^{2+}]i$. We performed $[Ca^{2+}]i$ measurements using extracellular solutions containing $Na^+$ and compared them with experiments that used standard extracellular solutions in which all but 1 mM of extracellular $Na^+$ was replaced by choline and leaving extracellular $K^+$ at 2.8 mM. These ionic conditions are the same as those used in experiments shown in Figures 6C and 6D, which will likely keep the membrane potential of HEK-293 cells around −45 mV (see Figure 6C), thereby providing significant driving force for $Ca^{2+}$ influx. While both experimental protocols would allow TRPM4b to activate in a $[Ca^{2+}]i$-dependent manner following receptor-mediated $Ca^{2+}$ release and subsequent $Ca^{2+}$ influx through store-operated mechanisms, the cells would be expected to strongly depolarize in high $Na^+$-containing media but less so in the choline-based solutions.

Figures 6E and 6F illustrate the average changes in $[Ca^{2+}]i$ obtained in both wt and TRPM4b-overexpressing HEK-293 cells using $Na^+$- and choline-based extracellular solutions (n = 7–11). Although TRPM4b-overexpressing cells display a slightly attenuated plateau phase of elevated $[Ca^{2+}]i$ compared with wt HEK-293 cells, this effect is not very dramatic. This is not surprising, since wt HEK-293 cells possess endogenous TRPM4b channels that are capable of depolarizing the cells (see Figure 5D). However, the plateau phase of elevated $[Ca^{2+}]i$ is markedly enhanced in both cell types when $Na^+$ is replaced by choline, consistent with the notion that the more hyperpolarized membrane potential produced by the choline-based solution provides for a stronger driving force for $Ca^{2+}$ influx. In the absence of ATP, the

Table 1. $Ca^{2+}$-Activated Cation Channels

| Tissue/Cell | Conductance | Permeant Ions | $Ca^{2+}$ | Sensitivity | Reference |
|---|---|---|---|---|---|
| Human monocytes (U937) | 18 pS | $Na^+$, $K^+$ | No | $[Ca^{2+}]i \geq 100$ nM | Floto et al., 1997 |
| Mouse neuroblastoma | 22 pS | $Cs^+$, $K^+$, $Li^+$, $Na^+$ | No | $K_D = 1$ μM | Yellen, 1982 |
| Mouse collecting duct cells | 23 pS | $Cs^+$, $K^+$, $Li^+$, $Na^+$ | No | $[Ca^{2+}]i \geq 1$ μM | Korbmacher et al., 1995 |
| Rat collecting duct cells | 28 pS | $Cs^+$, $K^+$, $Li^+$, $Na^+$ | No | $K_D = 5$ μM | Nonaka et al., 1995 |
| Guinea pig cochlear hair cells | 25 pS | $K^+$, $Na^+$ | No | $[Ca^{2+}]i \geq 100$ nM | Van den Abbeele et al., 1994 |
| Rabbit smooth muscle cells | 28 pS | $Na^+$ | No | $[Ca^{2+}]i \geq 100$ nM | Wang et al., 1993 |
| Rat astrocytes | 35 pS | $K^+$, $Na^+$, $Li^+$ | No | $K_D = 310$ nM | Chen and SImard, 2001 |
| Chick dorsal root ganglion | 38 pS | $K^+$, $Na^+$ | No | $K_D = 400$ nM | Razani-Boroujerdi and Partridge, 1993 |
| Guinea pig cardiac myocytes | 15 pS | $Cs^+$, $K^+$, $Li^+$, $Na^+$ | n.d. | $K_D = 1.2$ μM | Ehara et al., 1988 |
| Rat cardiac myocytes | 30 pS | $K^+$, $Na^+$ | n.d. | $[Ca^{2+}]i \geq 1$ μM | Colquhoun et al., 1981 |
| Gerbil cochlear epithelial cells | 27 pS | $K^+$, $Na^+$ | n.d. | $[Ca^{2+}]i \geq 100$ nM | Chiba and Marcus, 2000 |
| Mouse pancreatic acinar cells | 30 pS | $K^+$, $Na^+$ | n.d. | $[Ca^{2+}]i \geq 1$ μM | Maruyama and Petersen, 1982 |

$Ca^{2+}$-activated nonselective cation channels in various cells and tissues exhibiting characteristics similar to TRPM4. Listed properties include single-channel conductance, permeability to monovalent cations, permeation of $Ca^{2+}$ (n.d. = not determined), sensitivity to $[Ca^{2+}]i$, and reference.

choline-based extracellular solution by itself had only a small $Ca^{2+}$-mobilizing effect that manifested itself as a delayed smooth wave of increased $[Ca^{2+}]i$ of ~20–90 nM, which was subtracted from the ATP-stimulated responses obtained in choline-based media. From these experiments we conclude that the plateau phase of elevated $[Ca^{2+}]i$ in both wt and TRPM4b-overexpressing HEK-293 are modulated by membrane potential changes in that the TRPM4b-mediated depolarization exerts negative feedback control on $Ca^{2+}$ influx.

## Discussion

We have cloned and characterized TRPM4b, a member of the TRPM subfamily of proteins (Montell et al., 2002a), which is widely expressed in both excitable and nonexcitable cells. TRPM4b forms homomultimers when overexpressed in HEK-293 cells and produces a $Ca^{2+}$-activated nonselective (CAN) cation channel of 25 pS unitary conductance that is directly activated by $[Ca^{2+}]i$ at or above ~300 nM and which conducts monovalent cations such as $Na^+$ and $K^+$, without significant permeation of $Ca^{2+}$ itself. Endogenous CAN channels with essentially identical properties are observed in wt HEK-293 cells, suggesting that homomultimeric TRPM4b channels are important contributors to TRPM4b function in a cellular context. Both endogenous and overexpressed TRPM4b are activated following receptor-mediated $Ca^{2+}$-mobilization, suggesting that TRPM4b channels underlie a regulatory mechanism that controls the magnitude of $Ca^{2+}$ influx by modulating the membrane potential and with it the driving force for $Ca^{2+}$ entry through other $Ca^{2+}$-permeable pathways.

The TRPM4b protein described in the present study is closely related to the TRPM4a protein that recently has been proposed to be a constitutively active cation channel mediating $Ca^{2+}$ entry when expressed in HEK-293 cells (Xu et al., 2001). The two proteins are derived from alternatively spliced transcripts of the same gene, with the present TRPM4b predicted protein including an additional 174 amino acids at the N-terminal region. In contrast to Xu et al.'s findings for TRPM4a, we find that TRPM4b is neither constitutively active nor does it seem to be significantly permeable to divalent cations. Rather, the longer TRPM4b is activated by elevated levels of $[Ca^{2+}]i$ and is permeable only to monovalent ions. It is not clear whether the additional amino acids at the N terminus of TRPM4b are responsible for the apparent differences in functional properties of the two proteins. While it is possible that the differences in the N terminus might affect the activation mechanisms being constitutive versus $Ca^{2+}$-dependent, it seems less likely that alterations in this region would affect the channel's pore selectivity. As in other ion channels, the pore region of TRPM4b is thought to reside between transmembrane-spanning domains 5 and 6, and this region is identical in both versions of TRPM4. If the shorter TRPM4 indeed is a constitutively active ion channel with similar selectivity as the longer one, then it is conceivable that the excessive $Na^+$ influx through TRPM4a homomultimers could lead to secondary alterations of the cell's mechanisms that regulate $Ca^{2+}$ homeostasis, e.g., by enhanced $Na^+/Ca^{2+}$ exchange.

The activation of TRPM4b is mediated by an elevation of $[Ca^{2+}]i$ above resting levels with a half-maximal effective concentration of ~300–400 nM when perfusing cells with buffered intracellular solutions. Thus, TRPM4b can be activated by $[Ca^{2+}]i$ in a concentration range that is physiologically achieved by $Ca^{2+}$-mobilizing receptor agonists. Indeed, we observed TRPM4b activity during $[Ca^{2+}]i$ changes induced by the purinergic receptor agonist ATP in both wt and TRPM4b-overexpressing HEK-293 cells. Importantly, TRPM4b can be gated in a cell-free context when exposing the cytosolic side of inside-out membrane patches to elevated $Ca^{2+}$ concentrations, suggesting that TRPM4b is directly gated by increased $[Ca^{2+}]i$. Thus, TRPM4b can be classified as a $Ca^{2+}$-activated nonselective (CAN) cation channel.

CAN channels are found in a variety of electrically excitable and nonexcitable cells. Despite the abundance of CAN channels in various tissues and cell lines, the molecular nature of any CAN has remained elusive. Although some of the TRP channels have been suggested to be activated by $Ca^{2+}$, this effect may have been caused indirectly, since modulatory effects of $Ca^{2+}$ on a variety of TRP channels have been observed. So far, no other TRP channel has been demonstrated to be directly gated by elevated $Ca^{2+}$ in a cell-free environment. Table 1 lists some of the cell types that have been

reported to possess endogenous CAN channels with broadly similar features as TRPM4b in terms of single-channel conductance and $Ca^{2+}$ dependence. Slight differences in these parameters between the native channels and TRPM4b may reflect species differences and/or differences in experimental conditions. Although more detailed comparative studies will be required to unambiguously identify some of these cation channels as TRPM4, the broad distribution of this protein makes it a good candidate to encode at least some of these channels.

Since TRPM4b does not conduct significant $Ca^{2+}$, its physiological impact on $Ca^{2+}$ signaling depends on the cellular context it is expressed in. In electrically nonexcitable cells that lack voltage-dependent $Ca^{2+}$ channels, significant activation of TRPM4b following a rise in $[Ca^{2+}]i$ would tend to reduce $Ca^{2+}$ influx by the depolarization-mediated decrease in driving force for $Ca^{2+}$ entry. In these cells, TRPM4b may act in concert with $K^+$ and $Cl^-$ channels to control $[Ca^{2+}]i$ oscillations through oscillatory changes in membrane potential. In electrically excitable cells such as neurons or cardiac myocytes, TRPM4b-mediated depolarizations might contribute to the frequency and/or duration of action potentials, thereby supporting $Ca^{2+}$ influx through voltage-gated $Ca^{2+}$ channels.

## Experimental Procedures

### Cloning and Sequence Analysis of TRPM4b

The genetrapper II solution hybridization method (Life Technologies) was used to isolate several TRPM4 cDNAs. Three rounds of screening with three different human cDNA libraries were performed: 13 PCR-positive colonies were obtained from the kidney library, all containing 3′ fragments of TRPM4 cDNAs. Further 5′ sequence was obtained from the spleen library. Using this supplementary 5′ segment to design new fishing oligonucleotides, another eight PCR-positive clones were isolated from a prostate library with a single clone containing the longest ORF, coding for TRPM4b. No splice variants of TRPM4 were observed based on sequence analysis of the 5′ ends of several near-full-length clones, suggesting that the TRPM4b is the predominant transcript in prostate, spleen, and kidney tissues.

### Northern Blot Analysis

Single-stranded probes were constructed with the *NheI*/*EcoRI*/*KpnI* 1 kb fragment of the human TRPM4 3′ end. FirstChoice™ Northern Blot for human tissue were obtained from Ambion (Austin, TX), and for the cell lines, 3 μg of polyA RNA per lane were used. The dUTP-labeled RNA probe was generated using a T7-directed RNA probe synthesis kit from Ambion. All hybridizations were performed according to the manufacturer's protocols.

### Protein Methods

Full-length TRPM4b cDNA was cloned into a modified version of the pCDNA4/TO vector (Invitrogen) with an N-terminal Flag epitope tag. The correct sequence of the full-length Flag-TRPM4b expression construct was confirmed by DNA sequencing. The Flag-TRPM4b cDNA in pCDNA4/T0 was electroporated into HEK-293 cells previously transfected with the pCDNA6/TR construct for Tet-repressor expression. Cells were placed under zeocin selection, and zeocin-resistant clones were screened for tetracycline-inducible expression of the Flag-tagged TRPM4b protein. Cell surface iodination with $Na^{125}I$ (1 mCi) (Amersham Pharmacia Biotech, Piscataway, NJ) was carried out by the lactoperoxidase method. For immunoprecipitation, cells ($10^7$/ml) were lysed for 30 min at 4°C in Tris buffer (pH 7.5) containing 0.5% Triton X-100 (Bio-Rad, Hercules, CA) and protease inhibitors. The Flag-tagged proteins were immunoprecipitated from cleared lysate by an anti-Flag antibody (Sigma, St. Louis, MO). In other experiments, anti-Cbl antibodies (Santa-Cruz Biotechnology, Santa-Cruz, CA) and anti-V5 tag (Invitrogen, Carlsbad, CA) were used. The immunoprecipitated proteins were resolved by 6% SDS-PAGE and visualized by Enhanced Chemiluminescence (Amersham Pharmacia Biotech).

### Cell Culture and Electrophysiology

Wild-type and tetracycline-inducible HEK-293 Flag-TRPM4-expressing cells were cultured at 37°C/5% $CO_2$ in DMEM supplemented with 10% FBS and 2 mM glutamine. The medium was supplemented with blasticidin (5 μg/ml; Invitrogen) and zeocin (0.4 mg/ml; Invitrogen). For most experiments, cells were resuspended in media containing 1 μg/ml tetracycline (Invitrogen) 18–22 hr before experiments, except for experiments shown in Figure 3C, where cells were exposed to tetracycline for 24–28 hr. For patch-clamp experiments, cells were kept in a standard Ringer's solution (in mM): NaCl 145, KCl 2.8, $CaCl_2$ 1, $MgCl_2$ 2, glucose 10, HEPES·NaOH 10 (pH 7.2). In some experiments, this solution was modified such that all but 1 mM of NaCl was replaced by choline-Cl (choline-based solution). In experiments where ATP was used, it was added at 1 mM of the $Mg^{2+}$ salt, and extracellular $Ca^{2+}$ concentration was raised to 2 mM. The standard pipette-filling solutions contained (in mM): K-glutamate 145, NaCl 8, $MgCl_2$ 1, K-BAPTA 10 (pH 7.2) adjusted with KOH. In some experiments, $[Ca^{2+}]i$ was buffered to 0.1–1 μM by 10 mM BAPTA and appropriate concentrations of $CaCl_2$ or left unbuffered. For inside-out single-channel recordings, the patch was excised into a similar solution, except that KCl was used instead of K-glutamate. All reagents were purchased from Sigma and dissolved in the standard intracellular solution. Patch-clamp experiments were performed in the whole-cell configuration at 21°C–25°C. Data was acquired with "Pulse" software controlling an EPC-9 amplifier (HEKA, Lambrecht, Germany). Voltage ramps of 50 ms duration spanning the voltage range of −100 to +100 mV were delivered from a holding potential of 0 mV at a rate of 0.5 Hz over a period of 200 to 400 s. When applicable, voltages were corrected for liquid junction potentials. Currents were filtered at 2.9 kHz and digitized at 100 μs intervals. For display purposes, ramp currents were digitally filtered to 2 kHz. Reversal potentials were determined from ramp current records that were corrected for linear leak (assessed at −80 mV) by measuring the voltage of the first data point that crossed the zero-current level. Capacitive currents and series resistance were determined and corrected before each voltage ramp. The low-resolution temporal development of currents at a given potential was extracted from the individual ramp current records by measuring the current amplitudes at voltages of −80 mV or +80 mV. Single-channel recordings were performed in the inside-out configuration, and currents were filtered and sampled as above. For display purposes, single-channel data records were digitally filtered and down-sampled to 100 Hz.

### Calcium Measurements

The cytosolic calcium concentration of individual patch-clamped or intact cells was monitored at a rate of 5 Hz with a photomultiplier-based system using a monochromatic light source tuned to excite fura-2 fluorescence at 360 and 390 nm for 20 ms each. Emission was detected at 450–550 nm with a photomultiplier, whose analog signals were sampled and processed by X-Chart software (HEKA, Lambrecht, Germany). Fluorescence ratios were translated into free intracellular calcium concentration based on calibration parameters derived from patch-clamp experiments with calibrated calcium concentrations. In patch-clamp experiments, fura-2 was added to the standard intracellular solution at 100 μM. Ester loading of intact cells was performed by incubating cells for 30–45 min in standard solution supplemented with 5 μM fura-2-AM. Local perfusion of individual cells with ATP was achieved through a wide-tipped, pressure-controlled application pipette (3 μm diameter) placed at a distance of 30 μm from the cell under investigation.

### Acknowledgments

We thank Mahealani Monteilh-Zoller for technical assistance. This work was supported in part by the following grants from the National Institutes of Health: R01AI46734 to J.-P.K., R01NS40927 and

R01AI50200 to R.P., and R01GM64091 to A.M.S. P.L was supported by a fellowship from Human Frontier Science Program Organization.

Received: December 20, 2001
Revised: March 15, 2002

## References

Chen, M., and Simard, J.M. (2001). Cell swelling and a nonselective cation channel regulated by internal $Ca^{2+}$ and ATP in native reactive astrocytes from adult rat brain. J. Neurosci. *21*, 6512–6521.

Chiba, T., and Marcus, D.C. (2000). Nonselective cation and BK channels in apical membrane of outer sulcus epithelial cells. J. Membr. Biol. *174*, 167–179.

Clapham, D.E., Runnels, L.W., and Strubing, C. (2001). The TRP ion channel family. Nat. Rev. Neurosci. *2*, 387–396.

Colquhoun, D., Neher, E., Reuter, H., and Stevens, C.F. (1981). Inward current channels activated by intracellular Ca in cultured cardiac cells. Nature *294*, 752–754.

Ehara, T., Noma, A., and Ono, K. (1988). Calcium-activated nonselective cation channel in ventricular cells isolated from adult guinea-pig hearts. J. Physiol. (Lond.) *403*, 117–133.

Elliott, A.C. (2001). Recent developments in non-excitable cell calcium entry. Cell Calcium *30*, 73–93.

Floto, R.A., Somasundaram, B., Allen, J.M., and Mahaut-Smith, M.P. (1997). Fcgamma receptor I activation triggers a novel $Ca^{2+}$-activated current selective for monovalent cations in the human monocytic cell line, U937. J. Biol. Chem. *272*, 4753–4758.

Gao, Z., Chen, T., Weber, M.J., and Linden, J. (1999). $A_{2B}$ adenosine and $P2Y_2$ receptors stimulate mitogen-activated protein kinase in human embryonic kidney-293 cells. Cross-talk between cyclic AMP and protein kinase C pathways. J. Biol. Chem. *274*, 5972–5980.

Harteneck, C., Plant, T.D., and Schultz, G. (2000). From worm to man: three subfamilies of TRP channels. Trends Neurosci. *23*, 159–166.

Hofmann, T., Schaefer, M., Schultz, G., and Gudermann, T. (2000). Transient receptor potential channels as molecular substrates of receptor-mediated cation entry. J. Mol. Med. *78*, 14–25.

Korbmacher, C., Volk, T., Segal, A.S., Boulpaep, E.L., and Fromter, E. (1995). A calcium-activated and nucleotide-sensitive nonselective cation channel in M-1 mouse cortical collecting duct cells. J. Membr. Biol. *146*, 29–45.

Maruyama, Y., and Petersen, O.H. (1982). Single-channel currents in isolated patches of plasma membrane from basal surface of pancreatic acini. Nature *299*, 159–161.

McKemy, D.D., Neuhausser, W.M., and Julius, D. (2002). Identification of a cold receptor reveals a general role for TRP channels in thermosensation. Nature, in press. Published online February 10, 2002. 10.1038/nature719

Montell, C., Birnbaumer, L., Flockerzi, V., Bindels, R.J., Bruford, E.A., Caterina, M.J., Clapham, D.E., Harteneck, C., Heller, S., Julius, D., et al. (2002a). A unified nomenclature for the superfamily of TRP cation channels. Mol. Cell *9*, 229–231.

Montell, C., Birnbaumer, L., and Flockerzi, V. (2002b). The TRP channels, a remarkably functional family. Cell *108*, 595–598.

Nadler, M.J., Hermosura, M.C., Inabe, K., Perraud, A.L., Zhu, Q., Stokes, A.J., Kurosaki, T., Kinet, J.P., Penner, R., Scharenberg, A.M., and Fleig, A. (2001). LTRPC7 is a Mg·ATP-regulated divalent cation channel required for cell viability. Nature *411*, 590–595.

Nonaka, T., Matsuzaki, K., Kawahara, K., Suzuki, K., and Hoshino, M. (1995). Monovalent cation selective channel in the apical membrane of rat inner medullary collecting duct cells in primary culture. Biochim. Biophys. Acta *1233*, 163–174.

Parekh, A.B., and Penner, R. (1997). Store depletion and calcium influx. Physiol. Rev. *77*, 901–930.

Partridge, L.D., Muller, T.H., and Swandulla, D. (1994). Calcium-activated non-selective channels in the nervous system. Brain Res. Brain Res. Rev. *19*, 319–325.

Peier, A.M., Moqrich, A., Hergarden, A.C., Reeve, A.J., Andersson, D.A., Story, G.M., Earley, T.J., Dragoni, I., McIntyre, P., Bevan, S., and Patapoutian, A. (2002). A TRP channel that senses cold stimuli and menthol. Cell *108*, 705–715. Published online February 11, 2002 10.1016/S0092867402006529.

Perraud, A.L., Fleig, A., Dunn, C.A., Bagley, L.A., Launay, P., Schmitz, C., Stokes, A.J., Zhu, Q., Bessman, M.J., Penner, R., et al. (2001). ADP-ribose gating of the calcium-permeable LTRPC2 channel revealed by Nudix motif homology. Nature *411*, 595–599.

Razani-Boroujerdi, S., and Partridge, L.D. (1993). Activation and modulation of calcium-activated non-selective cation channels from embryonic chick sensory neurons. Brain Res. *623*, 195–200.

Runnels, L.W., Yue, L., and Clapham, D.E. (2001). TRP-PLIK, a bifunctional protein with kinase and ion channel activities. Science *291*, 1043–1047.

Sano, Y., Inamura, K., Miyake, A., Mochizuki, S., Yokoi, H., Matsushime, H., and Furuichi, K. (2001). Immunocyte $Ca^{2+}$ influx system mediated by LTRPC2. Science *293*, 1327–1330.

Siemen, D. (1993). Nonselective cation channels. EXS *66*, 3–25.

Thorn, P., and Petersen, O.H. (1993). Nonselective cation channels in exocrine gland cells. EXS *66*, 185–200.

Van den Abbeele, T., Tran Ba Huy, P., and Teulon, J. (1994). A calcium-activated nonselective cationic channel in the basolateral membrane of outer hair cells of the guinea-pig cochlea. Pflugers Arch. *427*, 56–63.

Wang, Q., Hogg, R.C., and Large, W.A. (1993). A monovalent ion-selective cation current activated by noradrenaline in smooth muscle cells of rabbit ear artery. Pflugers Arch. *423*, 28–33.

Xu, X.Z., Moebius, F., Gill, D.L., and Montell, C. (2001). Regulation of melastatin, a TRP-related protein, through interaction with a cytoplasmic isoform. Proc. Natl. Acad. Sci. USA *98*, 10692–10697.

Yellen, G. (1982). Single $Ca^{2+}$-activated nonselective cation channels in neuroblastoma. Nature *296*, 357–359.

## Accession Numbers

The GenBank accession number for TRPM4b is AF497623.